AGU PUBLICATIONS

Geophysical Research Letters

RESEARCH LETTER
10.1002/2017GL075674

Key Points:
- We introduce a new scheme to forecast winter European and Mediterranean precipitation using cluster analysis and autumn precursors
- Clustering analysis identified three dominant patterns of precipitation anomalies across Europe and the Mediterranean
- Comparison of forecasts with NMME model forecasts and CCA-based forecasts reveals that the clustering forecasts have the highest accuracy

Supporting Information:
- Supporting Information S1

Correspondence to:
J. Cohen,
jcohen@aer.com

Citation:
Totz, S., Tziperman, E., Coumou, D., Pfeiffer, K., & Cohen, J. (2017). Winter precipitation forecast in the European and Mediterranean regions using cluster analysis. *Geophysical Research Letters*, *44*, 12,418–12,426. https://doi.org/10.1002/2017GL075674

Received 12 JUL 2017
Accepted 16 NOV 2017
Accepted article online 21 NOV 2017
Published online 17 DEC 2017

Winter Precipitation Forecast in the European and Mediterranean Regions Using Cluster Analysis

Sonja Totz[1,2], Eli Tziperman[3], Dim Coumou[1,4], Karl Pfeiffer[5], and Judah Cohen[5]

[1]Potsdam Institute for Climate Impact Research, Potsdam, Germany, [2]Department of Physics, University of Potsdam, Potsdam, Germany, [3]Department of Earth and Planetary Sciences, and School of Engineering and Applied Sciences, Harvard University, Cambridge, MA, USA, [4]Department of Water and Climate Risk, Institute for Environmental Studies, VU University, Amsterdam, Netherlands, [5]Atmospheric and Environmental Research, Inc., Lexington, MA, USA

Abstract The European climate is changing under global warming, and especially the Mediterranean region has been identified as a hot spot for climate change with climate models projecting a reduction in winter rainfall and a very pronounced increase in summertime heat waves. These trends are already detectable over the historic period. Hence, it is beneficial to forecast seasonal droughts well in advance so that water managers and stakeholders can prepare to mitigate deleterious impacts. We developed a new cluster-based empirical forecast method to predict precipitation anomalies in winter. This algorithm considers not only the strength but also the pattern of the precursors. We compare our algorithm with dynamic forecast models and a canonical correlation analysis-based prediction method demonstrating that our prediction method performs better in terms of time and pattern correlation in the Mediterranean and European regions.

Plain Language Summary We have applied a new forecasting technique to the problem of seasonal prediction that involves machine learning. By recognizing related and reoccurring patterns in both the predictors and the predictands our new technique shows improved accuracy in predicting winter precipitation in the European and Mediterranean regions. Our demonstrated technique outperforms both statistical and dynamical models over comparable historical periods.

1. Introduction

European climate is characterized by four distinct climate zones: Mediterranean climate in southern Europe, continental climate in eastern Europe, maritime climate in western Europe, and a hybrid maritime/continental climate in central Europe (Hess & Tasa, 2011). Those climate regions are sensitive to large-scale circulations of the atmosphere. Even relatively minor modifications of the general circulation results in shifts of the midlatitude storm tracks and substantial changes in the climate (Giorgi, 2006; Kröner et al., 2017; Lionello et al., 2006; Mbengue & Schneider, 2013). The Mediterranean climate is especially vulnerable to climate change due to its unique topography and geographical location and is therefore considered as one of the primary climate change hot spots since strong climate changes are projected in this region (Diffenbaugh & Giorgi, 2012; Dubrovsky et al., 2014; Giorgi, 2006; Intergovernmental Panel on Climate Change (IPCC), 2013). The Mediterranean climate is generally characterized by hot and dry summers as well as by mild winters, with winter rainfall more than 3 times larger than summer rainfall (Ducrocq et al., 2014; Flaounas et al., 2013). Winter rainfall is mostly determined by synoptic storms coming from the North Atlantic (Giorgi & Lionello, 2008). In general, the winter Mediterranean precipitation is related to the North Atlantic Oscillation (NAO) over its western areas, the East Atlantic (EA), and other patterns over its northern and eastern areas (Giorgi & Lionello, 2008; Kröner et al., 2017; Lionello et al., 2006; Mbengue & Schneider, 2013; Ullbrich et al., 2006). Other studies argue that also the El Niño Southern Oscillation (ENSO) affects precipitation in the Mediterranean region (Park & Leovy, 2004; Shaman & Tziperman, 2011). Both Park and Leovy (2004) as well as Shaman and Tziperman (2011) suggest that a Rossby wave train originating from the Pacific in autumn might affect the Mediterranean winter climate (Gurmy et al., 2012). Other potentially important factors are sea ice concentration and snow cover extent with Eurasian snow cover in autumn significantly correlating with the wintertime Arctic Oscillation and mean sea level pressure (Cohen & Jones, 2011; Furtado et al., 2016).

Hoerling et al. (2012) show that the Mediterranean region is already drying. In a time period between 1988 and 2008 the region had 10 of the 12 driest winter seasons (Hoerling et al., 2012). Anomalously high seasonal temperatures or low precipitation in the Mediterranean region have been recently observed decimating agricultural yields and causing damages up to hundreds of millions of dollars each year (Ducrocq et al., 2014). Future climate simulations project an even stronger trend toward drying (Giorgi, 2006; IPCC, 2013; Paeth et al., 2017; Xoplaki et al., 2004). Although it is well known that anthropogenic greenhouse gas forcing leads to enhanced warming in the Mediterranean region, there is uncertainty in projected changes in precipitation due to large internal variability and a relatively small forced signal (Hoerling et al., 2012; Mariotti et al., 2015). However, both Hoerling et al. (2012) and Mariotti et al. (2015) show that the probability distribution of future precipitation anomalies is shifted toward dryer conditions.

Early forecast techniques of seasonal drought like multimodel ensemble predictions, dynamical or statistical downscaling, and empirical forecast approaches could play an important role in mitigating possible future impacts. Examples for empirical forecast approaches are multiple linear regressions or canonical correlation analysis (CCA), which is a form of linear multiple regression applied to multivariate pattern predictands (Barnett & Preisenberger, 1987; Barnston et al., 1996; Chu et al., 2008; Doblas-Reyes et al., 2000; Eden et al., 2015; Hwang et al., 2001; Yatagai et al., 2014). However, global circulation models have little or no skill in predicting European precipitation during December-January-February (DJF) (Doblas-Reyes et al., 2009; Weisheimer & Palmer, 2014). Weisheimer and Palmer classify seasonal forecasts of wintertime rainfall over the Mediterranean region as only marginally useful for decision makers and policymakers (Weisheimer & Palmer, 2014). Likewise, previous empirical forecast approaches such as multiple linear regressions or CCA have essentially no skill over this region for predicting rainfall (Barnston & Smith, 1996; Eden et al., 2015). For example, Eden et al. developed a simple empirical system for predicting seasonal surface air temperature and precipitation across the globe using global and local atmospheric and oceanic fields (Eden et al., 2015). In particular, they used CO_2 concentration to predict the climate change signal and additional predictors describing large-scale modes of variability in the climate system (e.g., ENSO) to forecast the variability in the climate system. The hindcast-observation correlation for the time range 1961–2013 is generally low over the globe with some parts of northern Eurasia with positive skill. The mean correlation over Europe and the Mediterranean region is almost zero. Also Barnston et al. (1996) algorithm using CCA to forecast the global Northern Hemisphere has only weak skill over Europe and the Mediterranean region. Barnston et al. (1996) used reconstructed sea surface temperature (SST) data set as the only predictor to hindcast near-global SST and seasonal mean surface temperature and precipitation based on the 1950–1992 period. The hindcast skills for Europe are generally poor, and the average skill for DJF is roughly 0.1 for zero season lead time. The weak skills for Europe do not imply that the statistical methods are not suitable for seasonal forecasts. Possible reasons include also chosen predictors, the chosen predictor regions, or the chosen time lags.

Here we propose a novel empirical prediction system that is more skillful and hence could possibly ease the decision-making process of stakeholders interested in seasonal prediction (Barriopedro et al., 2011). The novelty of our method to forecast winter European and Mediterranean precipitation is that it accounts not only for the amplitude of predictors but also for the geographical patterns using clustering techniques. Similar to CCA, clusters in our algorithm were used to describe the dominant patterns of the precipitation anomalies over Europe and the Mediterranean region with the advantage that those states do not have to be orthogonal to each other. The forecast algorithm calculates precipitation anomalies in winter with the analyzed precursors in autumn.

2. Data and Methods

2.1. Data

In this study, we calculated detrended precipitation anomalies from a gridded data set of precipitation provided by the "European Climate Assessment and Data Set Project" (Haylock et al., 2008). This data set is on a 0.5° × 0.5° grid over the area between 25° to 75° latitude and −20° to 45° longitude for the winter time period (December-January-February, DJF) 1967 to 2016. The anomaly fields are smoothed using a Gaussian filter ($\sigma_x = 2.7, \sigma_y = 2.7$). In addition, we used several detrended precursor fields in autumn (September-October-November, SON) for the overlapping period 1996 to 2015, including sea ice concentration (**sic**) from the Met Office Hadley Centre (at 2.5° × 2.5°) for the area between 60° to 90° latitude and 0°

to 180° longitude. We further include snow cover extent (**sce**) provided by NOAA (Robinson et al., 2012) using the area between 30° to 60° latitude and 0° to 180° longitude. The choice of this area is motivated by the snow advance index, which computes the snow cover extent over the same area (Cohen & Jones, 2011). Furthermore, we include sea surface temperatures (**sst**) from the Met Office Hadley Centre (at $1^\circ \times 1^\circ$) using three different regions: the tropical Pacific (−40° to 20° latitude and 130° to 290° longitude), the North Atlantic (0° to 65° latitude and −35° to 6° longitude), and the Mediterranean region (30° to 50° latitude and −6° to 45° longitude) (Rayner et al., 2013). In addition, we include geopotential height (**gph**) at 500 mb using the area between −20° to 90° latitude and 0° to 360° longitude (Kalnay et al., 1996). The same area is used for sea level pressure (**slp**). Atmospheric data are from National Centers for Environmental Prediction (NCEP)/National Center for Atmospheric Research (NCAR; at $2.5^\circ \times 2.5^\circ$) (Kalnay et al., 1996). In addition, we calculated the ensemble model mean for nine models of hindcast experiments provided by the North American Multimodel Ensemble (NMME: CMC1-CanCM3, CMC2-CanCM4, NCAR-CESM1, NCEP-CFSv2, COLA-RSMAS-CCSM3, COLA-RSMAS-CCSM4, NASA-GMAO, IRI- ECHAMP4p5-DirectCoupled, and IRI-ECHAMP4p5-AnomalyCoupled) (Kirtman et al., 2014). NMME System Phase II data (https://www.earthsystemgrid.org/search.html?Project=NMME) were used in these analyses. The NMME is a multiagency project under the guidance of the United States National Oceanic and Atmospheric Administration (NOAA). The NMME System is designed to leverage coupled models from a number of United States and Canadian modeling centers in an ensemble of opportunity supporting seasonal forecasting experiments (Kirtman et al., 2014). NMME models are coupled to ocean models, and most of the NMME models have an ice component model. Some models use also a land component model including soil moisture and snow cover (Collins et al., 2005; De Witt, 2005; Gent et al., 2011; Merryfield et al., 2013; Saha et al., 2014). The real-time and retrospective forecasts are issued on the fifteenth of each month, for example, a November 2010 monthly mean forecast is the 0.5 month lead issued on 15 November 2010, and the December 2010 monthly mean forecast issued on 15 November is the 1.5 month lead and so on. The hindcast start times should include all 12 calendar months. However, the specific day of the month or the ensemble generation strategy is dedicated to the forecast provider. Hence, different models are initialized at a different start day, for example, the model CMC2-CanCAM5 initializes all ensemble models at the first of a month, whereas CFSv2 initializes all four members (0000, 0600, 1200, and 1800 UTC) every fifth day. In the present work we evaluated NMME forecasts issued on 15 November and 15 December for the DJF period.

2.2. Clustering-Based Forecast Approach

To obtain the prediction for the winter precipitation anomaly, we proceed as follows (further details as well as an example using a toy problem are provided in the supporting information, SI). We calculate the cluster structures by applying hierarchical clustering to the winter precipitation anomalies over the domain of interest. Hierarchical clustering (e.g., Cheng & Wallace, 1993; Feldstein & Lee, 2014; Horton et al., 2015; Kretschmer et al., 2017; Lee & Feldstein, 2013) is a common and powerful clustering analysis procedure. The precipitation anomaly at each season is arranged as a vector data point. The algorithm then constructs a hierarchy of clusters by merging one pair of nearest data points or clusters of points at each step (Wilks, 2011). Standard measures are used to determine when to stop the merging and therefore the appropriate number of clusters, N_{clusters} (Figure S3 in the SI).

Each cluster of winter precipitation anomalies groups together seasons with similar spatial patterns of precipitation, and their averages, the clusteroids, represent the most common spatial precipitation patterns. Next, we find the composites of the different autumn predictors (**SST**, **SCE**, **SIC**, etc) corresponding to a given cluster, by averaging the predictors over all autumn seasons (SON) for which the following winter precipitation anomaly is assigned to a given cluster. The predictor's composites of the *i*th cluster are combined into one composite ($\mathbf{COMPOSITE}_i = (\mathbf{SST}_i, \mathbf{SCE}_i, \mathbf{SIC}_i, \mathbf{etc})^T$) with $i = 1 \ldots N_{\mathrm{clusters}}$. We use bold upper case variable names to denote clusters and composites, and lower case bold variable names to denote time series data. Given the current state of the precursors, we now produce the prediction as follows. First, we find the projection of the state of the predictors averaged over the autumn of year t (and denoted $\mathbf{precursor}_{\mathrm{SON}}(t)$) on the predictor composites. Each combined predictor composite is associated with a precipitation cluster and therefore provides information about the amount and spatial structure of winter precipitation anomaly expected given the autumn predictor composite. This allows us to calculate the expected precipitation pattern due to the projection of the current state of predictors on each cluster. We expand the current precursor state in terms of the precursor composites as

$$\mathbf{precursor}_{\mathrm{SON}}(t) \approx \sum_{i=1}^{N_{\mathrm{clusters}}} a_i(t)\, \mathbf{COMPOSITE}_i. \tag{1}$$

The expansion may only be approximate because the composites are not necessarily a complete set of vectors. To find the expansion coefficients $a_i(t)$, we multiply equation (1) by precursor composite $\mathbf{COMPOSITE}_j$ and solve the equation for the coefficients $a_i(t)$ at every time step (year t) in the data using the SVD-based pseudoinverse (SI).

Finally, we sum the contributions to the precipitation due to all clusters, each multiplied by the projection of the current state of precursors, $a(i)$, to obtain the predicted total precipitation anomaly. For example, assuming that snow cover extent is the only predictor and assuming that the current autumn snow cover extent is a combination of two composites, corresponding to two specific precipitation clusters, then we expect the following winter precipitation to be a combination of those two precipitation cluster patterns. More generally, the precipitation forecast is given by

$$\mathbf{prcp}(t) = \sum_{i=1}^{N_{\text{clusters}}} a_i(t)\, \mathbf{PRCP}_i. \tag{2}$$

2.3. Canonical Correlation Analysis

CCA is a statistical technique that identifies the linear associations among two data sets of variables, that is, it relates variations in predictor fields to variations in predictand fields (Barnett & Preisenberger, 1987; Barnston et al., 1996; Wilks, 2011; Xoplaki et al., 2004). By construction, the identified linear combinations of variables are maximally correlated. We apply this method in order to compare our algorithm with the already established pattern-based method CCA. For comparison, we use the same input predictors as used for the clustering-based method.

3. Results and Discussion

3.1. Clusters and Composites

The appropriate number of clusters is found to be three, based on standard measures (Figure S3), and the clusters are shown in Figure 1, ordered by their frequency: 48% of the winter seasons fall within cluster 1 (Figure 1a), 28% within cluster 2 (Figure 1b), and 24% in cluster 3 (Figure 1c).

To explore the possible precursors associated with each cluster pattern, composites for sea ice concentration (**sic**), snow cover extent (**sce**), sea surface temperature in the Mediterranean region ($\mathbf{sst}_{\text{Medi}}$), Atlantic ($\mathbf{sst}_{\text{Atl}}$), and tropics ($\mathbf{sst}_{\text{Tropics}}$), and geopotential height (**gph**) and sea level pressure (**slp**) are calculated (Figures S5–S7). Examples are shown for the precursors **sic**, **sce**, $\mathbf{sst}_{\text{Medi}}$, and $\mathbf{sst}_{\text{Atl}}$ for cluster two, because (as shown below) those three precursors give the best forecast skill across all clusters (Figure 2). We calculated the precursor anomalies to show the different patterns. In the algorithm we do not use precursor anomalies but the actual precursor values. The prediction of seasonal precipitation anomalies is then obtained by the procedure that is described in section 2.3 and schematically shown in Figure S8.

All three clusters of precipitation anomalies exhibit distinct properties: Cluster 1 reveals a weak drying structure with positive precipitation anomalies across the north of Europe, whereas cluster 2 corresponds primarily to a positive NAO (Figure 1). The corresponding composites of cluster 2 reveal patterns, which are associated with a positive NAO pattern. The composites of cluster 3 reveal patterns that are associated with negative NAO pattern. The typical patterns of the precursors for a positive NAO pattern are shown in Figure 2: **sce** exhibits more negative snow anomalies, **sic** exhibits more positive sea ice concentration anomalies, $\mathbf{sst}_{\text{Medi}}$ exhibits more positive temperature anomalies, and $\mathbf{sst}_{\text{Atl}}$ shows a tripole temperature anomaly pattern.

Other precursors were investigated but found to be less skillful than the set of precursors **sic**, **sce**, $\mathbf{sst}_{\text{Medi}}$, and $\mathbf{sst}_{\text{Atl}}$ achieving the highest skill score.

The physical mechanisms of the three different precursors leading to more precipitation are the following: The Mediterranean Sea is a major moisture source (Lionello et al., 2006). In late October and early November low pressure systems develop in the Mediterranean region due to the convergence of maritime tropical air from the Atlantic, maritime polar air from the North Atlantic and northwest Europe, maritime Arctic and continental Arctic air from the Arctic and northern Russia, and continental tropical air from the Sahara. The cyclogenesis is energized by the sea surface temperature that enhances the evaporation and atmospheric transport and brings the winter precipitation (Smithson et al., 2013). The Alps deflect the water saturated wind, which can lead to more rainfall.

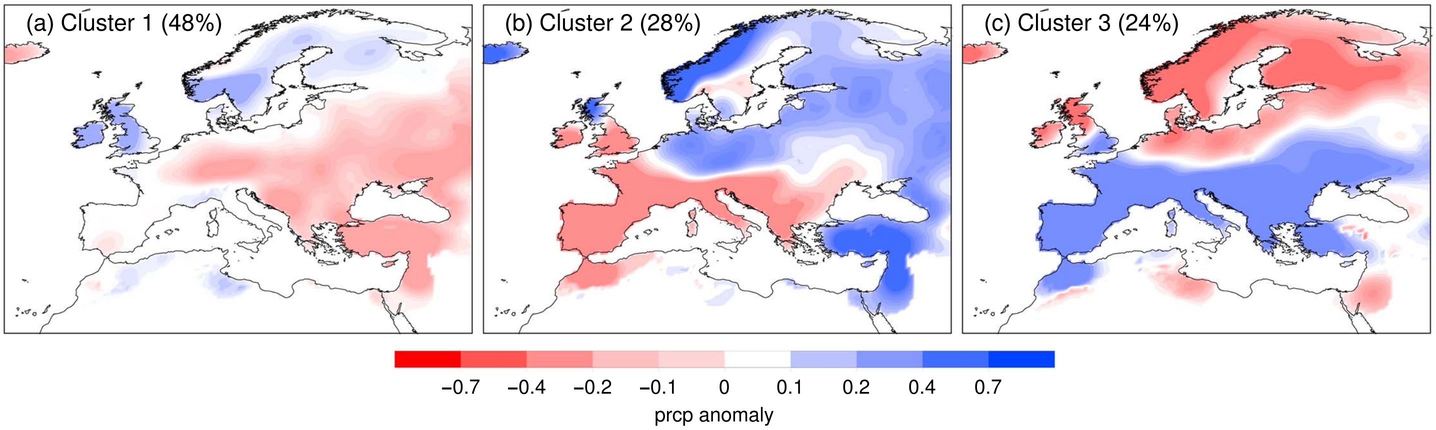

Figure 1. Clusters of precipitation anomalies for the Mediterranean region, ordered by their frequency: (a) Cluster 1 has a frequency of 48%, (b) Cluster 2 has a frequency of 28%, and (c) Cluster 3 has a frequency of 24%. The clusters are calculated by using hierarchical clustering and represent the dominant patterns of the precipitation anomalies over Europe and the Mediterranean region.

Positive North Atlantic SST anomalies across the midlatitudes and negative North Atlantic SST anomalies in the subtropics lead to a southward shift of storm tracks from western Europe toward the Mediterranean region. The combination of both the shift of the storm tracks and the local cyclogenesis produces the spatial distribution of the precipitation pattern (positive precipitation anomalies over the western and central Mediterranean region) (Xoplaki et al., 2004).

Sea ice loss in September and October warms the atmosphere and leads to an increase of the geopotential height, which forces the jet stream southward over east Siberia. This southward shift of the jet stream is associated with a southward shift of the storm tracks leading to more Eurasian snow cover in October. In addition, the ice-free ocean contributes to an increased moisture flux in the atmosphere, which precipitates as snow southward over Siberia. The anomalously high Eurasian snow cover cools the surface, which increases the surface pressure and reduces the geopotential heights in the lower and middle troposphere. This planetary wave configuration enhances vertical wave propagation from the troposphere into the stratosphere, which weakens the stratosphere and results in a stratosphere warming event. In January and February, the lower stratospheric anomalies propagate downward into the troposphere inducing a negative phase of the NAO and hence a shift of the polar jet and storm track equatorward. These displacements are followed by a southward shift in the storm tracks across the midlatitudes and wetter conditions across the Mediterranean region (Cohen et al., 2014).

3.2. Forecast Using Cluster Analysis and Comparison With NMME and CCA

We calculated the cross-validated correlation between the hindcasts and observations of winter precipitation anomalies for the time period 1967 to 2016, as well as for the time period 1982 to 2010 in order to compare the results with the NMME ensemble that is provided for these years. We also present the results of the CCA empirical prediction method. Therefore, we used all data to compute clusters, composites, and finally, the hindcast, not using the data from the year we would like to predict. Such a prediction is performed for all years.

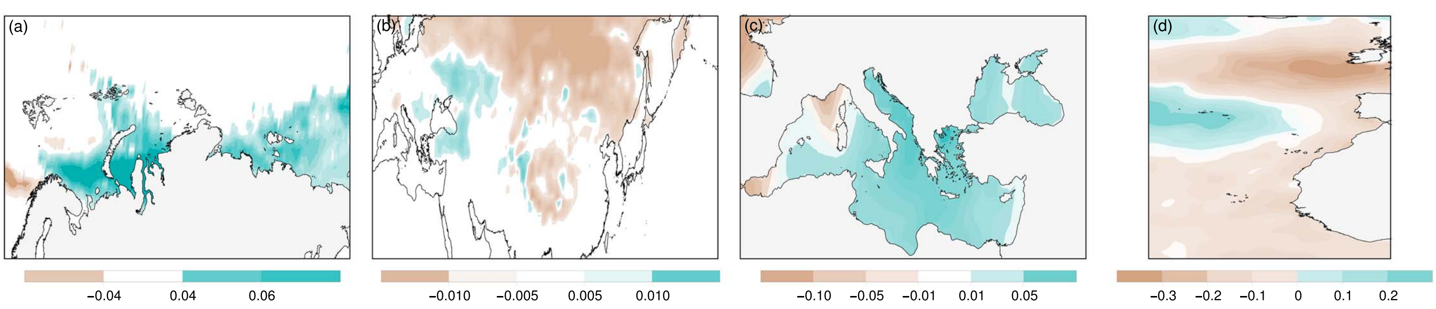

Figure 2. Composite mean of (a) sea ice concentration anomalies (**sic**), (b) snow cover extent anomalies (**sce**), (c) sea surface temperature anomalies in the Mediterranean region ($\mathbf{SST_{Medi}}$), and (d) sea surface temperature anomalies in the Atlantic region ($\mathbf{sst_{Atl}}$) over all autumn seasons assigned to cluster 2.

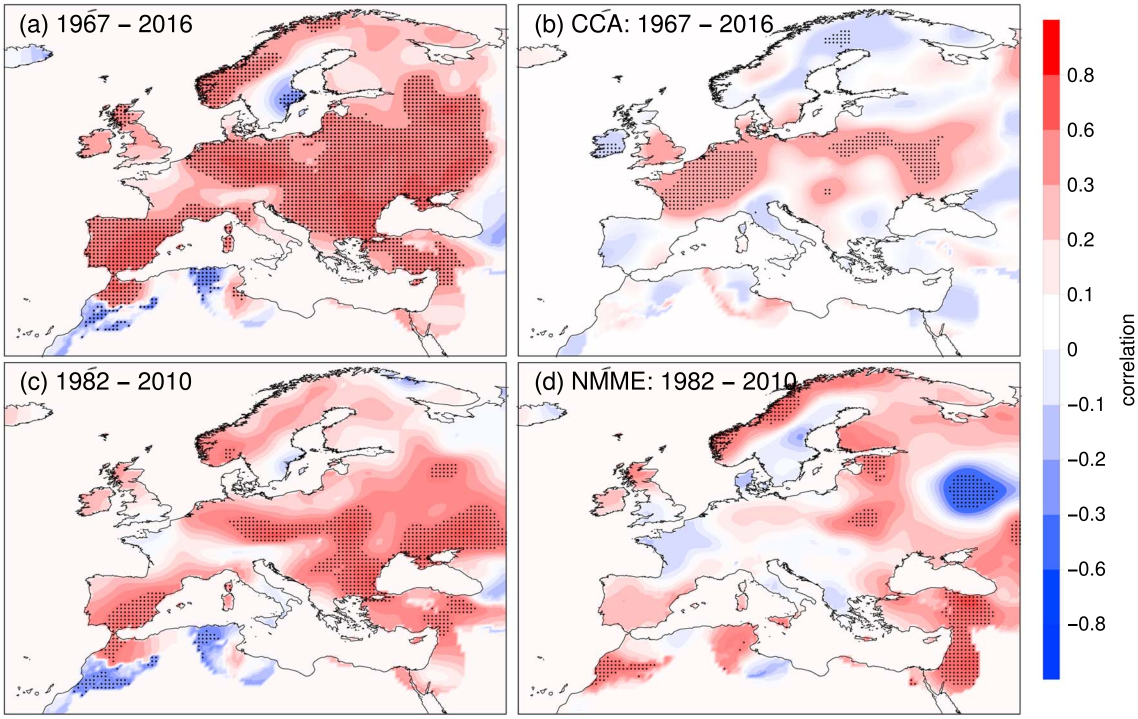

Figure 3. Precipitation forecast skill: (a) Cross validated correlation of the cluster-based hindcasts with observations for the year 1967–2016. (b) Same for the years 1982–2010. (c) Correlation of the NMME hindcasts for the years 1982–2010 with observations. Significant values ($P < 0.05$) according to the two-sided Student t test are shown in hatches. The cluster-based forecast performs better than the NMME models according to the cross-validated correlation.

Figure 3a shows the correlation for 1967 to 2016. Significant values ($P < 0.05$) according to the two-sided Student t test are shown in hatches. The correlation is in general positive, except for some parts of southern Sweden, Morocco, some regions of northern Algeria and Libya, as well as Georgia. The mean correlation is 0.22.

In contrast, the correlation between the CCA forecast and observations is mixed, with weak positive correlations in Central Europe, weak negative correlations at the margins of Europe and the Mediterranean region (Figure 3b), and a mean correlation of 0.05. Both the clustering and CCA approaches use the entire fields of the predictor and predictand, so one might expect them to perform similarly in terms of prediction skill. It is possible that the CCA performed less well because it is based on an empirical orthogonal function (EOF) expansion of the predictor and predictand, while the clusters represent common patterns that are not necessarily orthogonal and are thus less restrictive. We truncated the expansion of the predictor and predictand at three EOFs, although the skill with only two EOFs was nearly as good. There are possibly additional refinements to the CCA analysis that could have been used, but a more thorough analysis of the difference between the two approaches is beyond the scope of this paper.

The mean correlation of the NMME is 0.13 whereas the cluster-based method for the same time range exhibits a mean correlation of 0.20 (compare Figure 3c and Figure 3d). The cluster-based method has high skill over Central Europe, the Iberian Peninsula, and the Eastern Mediterranean. The NMME forecast shown in Figure 3d is based on an initialization on 15 November, while the CCA and cluster forecast, being based on seasonal averages, use data from September, October, and November. An NMME forecast similarly issued on 1 December is not available, and we present instead the results of the forecast issued on 15 December in the supporting information (Figure S10). The mean correlation in that case is 0.21, marginally better than that of the cluster analysis (0.20) although in this case the NMME prediction is based on December data and provides a December prediction, explaining the good skill in this case.

To investigate whether the Gaussian filter plays a role in our method, we show in Figure S9a the correlation for the precursors **sic**, **sce**, $\mathbf{sst}_{\mathrm{Medi}}$, and $\mathbf{sst}_{\mathrm{Atl}}$, but without using the Gaussian filter. It indicates that the correlation structure in central Europe is almost the same, but the Gaussian filter smooths the field leading to higher-correlation values. Most negative correlations vanish due to the smoothing. We also show

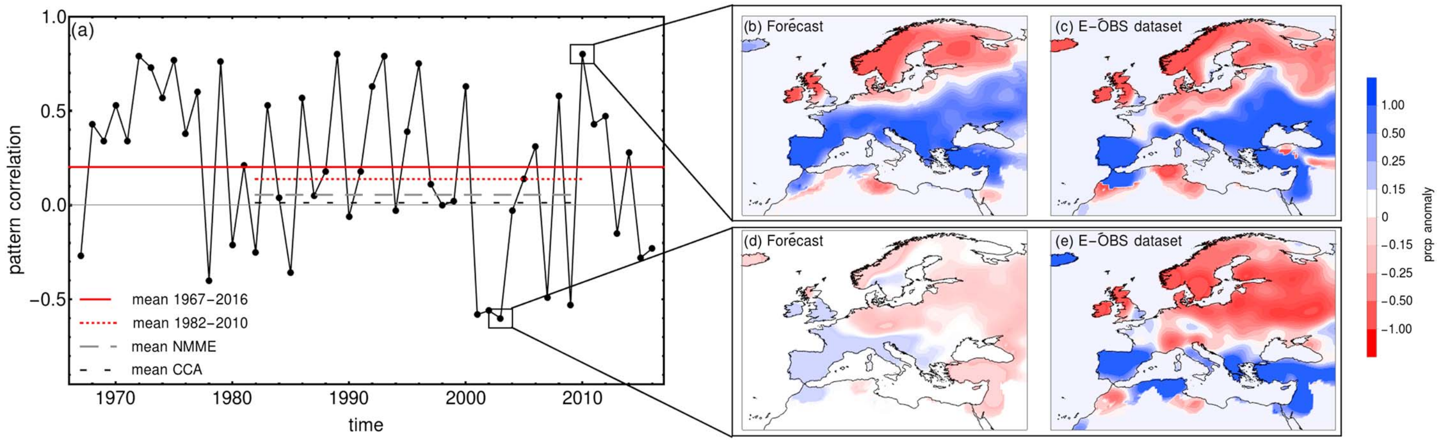

Figure 4. (a) Pattern correlation of the precipitation hindcasts and observations for the time range 1966 to 2016. The red solid line is the mean pattern correlation using the cluster-based method for the time range 1966–2016, the red dotted line is the mean pattern correlation using the cluster-based method for the time range 1982–2010, the black dashed line is the mean correlation of CCA for the time range 1967–2016, and the gray dashed line is the mean pattern correlation for the NMME models for the time range 1982–2010. (b)Precipitation hindcast for the best pattern correlation (2010). (c)Precipitation observation for year 2010. (d) Precipitation hindcast for the worst pattern correlation (2003). (e) Precipitation observation for year 2003.

correlations for other precursors $\mathbf{sst}_{\mathrm{Medi}}$ and $\mathbf{sst}_{\mathrm{Atl}}$ (Figure S9b), **sce** and **sic** (Figure S10c), and all three **sst** regions (Figure S9d) for the years 1967 to 2016.

Those plots reveal that the precursors $\mathbf{sst}_{\mathrm{Medi}}$ and $\mathbf{sst}_{\mathrm{Atl}}$ are likely more important in predicting **prcp anomalies** for southern, central, and eastern Europe, whereas the precursors **sic** and **sce** are more relevant to predict **prcp anomalies** in the southeastern and northern part of the Mediterranean region (compare Figure S9b and Figure S9c). While the $\mathbf{sst}_{\mathrm{Medi}}$ and $\mathbf{sst}_{\mathrm{Atl}}$ as precursors have moderate correlation with observational data, all three chosen sst regions have a low correlation and are less skillful than **sic** and **sce** in predicting **prcp anomalies**.

Finally, we compared the pattern correlation of our method for two different time ranges, 1967–2016 and 1982–2010, with the NMME and CCA (Figure 4). It is clearly visible that the pattern correlation using the cluster-based method is mostly positive for the longer time range with a mean pattern correlation of 0.20 and only for some years negative (black line in Figure 4a, red line represents the mean value). The dashed black line shows the mean pattern correlation of CCA with a mean pattern correlation of 0.01. The gray line exhibits the pattern correlation of the NMME with mean pattern correlation of 0.05, and the red dashed line exhibits the mean correlation of our hindcast method for the same time range mean pattern correlation of 0.18. Also the pattern correlation of NMME hindcasts issued on 15 December has a lower value (0.14) than the pattern correlation of the clustering method and is shown in Figure S10.

The results of the pattern correlations show that the cluster method resembles the observations more closely than NMME or CCA. We plotted the hindcast with the highest pattern correlation (year 2010) and the hindcast with the lowest pattern correlation (year 2003) as well as the observed data for those hindcasts (Figures 4b–4e).

Comparing the time plot of the clusters in Figure S3 with the pattern correlation plot (Figure 4a) reveals that clusters 2 and 3 have the best forecast skill. This likely stems from the fact that these clusters represent, respectively, a clear positive and negative NAO state, whereas the other one has a more complicated geographically distributed structure. This result suggests that extreme NAO states have better predictability than intermediate states.

4. Conclusion

This study presents a new cluster-based method to predict the precipitation anomalies in the European and Mediterranean regions using autumn precursors. The advantage of this approach is that both the magnitude and spatial structure of the precursors are utilized in generating the predictions. Applying hierarchical clustering, we identified three clusters describing the dominant patterns of the precipitation anomalies over Europe. From those clusters we calculated the composites of different precursors. To predict precipitation anomalies, we first computed the projection of the current state of the predictors onto the composites. Each predictor composite is associated with a precipitation cluster and provides information about the amount and spatial structure of winter precipitation expected given the autumn predictor composite. Thus, we can calculate the expected precipitation pattern by multiplying the projections of each cluster and summing up all products.

The cluster-based method achieves higher forecast skill in time and pattern correlation than a CCA-based prediction algorithm using the same predictor fields for both methods. In addition, the cluster-based method performs better than the NMME models in terms of pattern and time correlation.

Our algorithm achieves also higher skill than other empirical methods used in the past such as the multiregression model developed by Eden et al. (2015) or the CCA-based algorithm used by Barnston et al. (1996).

The method could be applied to temperature and precipitation anomalies in other regions or even possibly to forecast extreme weather.

Acknowledgments
The work was supported by the German Federal Ministry of Education and Research, grant 01LN1304A, (S. M. and D. C.). J. C. is supported by the National Science Foundation grants AGS-1303647 and PLR-1504361. E. T. is supported by the National Science Foundation climate dynamics program, grant AGS-1622985, and thanks to the Weizmann Institute for their hospitality during parts of this work. This work was supported by the National Science Foundation Large-Scale and Climate Dynamics Program (grants AGS-1303647 and AGS-1303604) and the National Science Foundation Division of Polar Programs (grant PLR-1504361). The research project resulted from S. M. visiting J. C., and S. M. would like to thank AER and Harvard for hosting. NCEP Reanalysis-derived data provided by the NOAA/OAR/ESRL PSD, Boulder, Colorado, USA, are available through their website at http://www.esrl.noaa.gov/psd/. SCE is available through the website https://climate.rutgers.edu/snowcover/. NMME System Phase II data are available through the website.

References

Barnston, A. G., & Smith, T. M. (1996). Specification and prediction of global surface temperature and precipitation from global SST using CCA. *Journal of Climate*, *9*(11), 2660–2697.

Barnston, A. G., Thiao, W., & Kumar, V. (1996). Long-lead forecast of seasonal precipitation in Africa using CCA. *Weather and Forecasting*, *11*, 506–520. https://doi.org/10.1175/1520-0434(1996)011<0506:LLFOSP>2.0.CO;2

Barriopedro, D., Fischer, E. M., Luterbacher, J., Trigo, R. M., & Garca-Herrera, R. (2011). The hot summer of 2010: Redrawing the temperature record map of Europe. *Science*, *332*(6026), 220–224. https://doi.org/10.1002/qj.464

Barnett, T. P., & Preisenberger, R. (1987). Origins and levels of monthly and seasonal forecast skill for United States surface air temperatures determined by canonical correlation analysis. *Monthly Weather Review*, *115*, 1825–1850. https://doi.org/10.1175/1520-0493(1987)115<1825:OALOMA>2.0.CO;2

Cheng, X., & Wallace, J. M. (1993). Cluster analysis of the Northern Hemisphere wintertime 500-hPa height field: Spatial patterns. *Journal of Atmospheric Sciences*, *50*(16), 2674–2696. https://doi.org/10.1175/1520-0469(1993)050<2674:CAOTNH>2.0.CO;2

Chu, J.-L., Kang, H., Tam, C.-Y., Park, C.-K., & Chen, C.-T. (2008). Seasonal forecast for local precipitation over northern Taiwan using statistical downscaling. *Journal of Geophysical Research*, *113*, D12118. https://doi.org/10.1029/2007JD009424

Cohen, J., & Jones, J. (2011). A new index for more accurate winter predictions. *Geophysical Research Letters*, *38*, L21701. https://doi.org/10.1029/2011GL049626

Cohen, J., Screen, J. A., Furtado, J. C., Barlow, M., Whittleston, D., Coumou, D., … Jones, J. (2014). Recent Arctic amplification and extreme mid-latitude weather. *Nature Geoscience*, *8*(9), 627–637.

Collins, W. D., Bitz, C. M., Blackmon, M. L., Bonan, G. B., Bretherton, C. S., Carton, J. A., … Smith, R. (2005). The Community Climate System Model version 3 (CCSM3). *Journal of Climate*, *19*, 2122–2143.

De Witt, D. G. (2005). Retrospective forecasts of interannual sea surface temperature anomalies from 1982 to present using a directly coupled atmosphere ocean general circulation model. *Monthly Weather Review*, *133*, 2972–2995.

Diffenbaugh, N. S., & Giorgi, F. (2012). Climate change hotspots in the CMIP5 global climate model ensemble. *Climatic change*, *114*(3–4), 813–822.

Doblas-Reyes, F. J., Déqué, M., & Piedelievre, J.-P. (2000). Multi-model spread and probabilistic seasonal forecasts in PROVOST. *Quarterly Journal of the Royal Meteorological Society*, *126*, 2069–2087. https://doi.org/10.1002/qj.49712656705

Doblas-Reyes, F. J., Weisheimer, A., Déqué, M., Keenlyside, N., McVean, M., Murphy, J. M., … Palmer, T. N. (2009). Addressing model uncertainty in seasonal and annual dynamical ensemble forecasts. *Quarterly Journal of the Royal Meteorological Society*, *135*, 1538–1559. https://doi.org/10.1002/qj.464

Dubrovsky, M., Hayes, M., Duce, P., Trnka, M., & Zara, P. (2014). Multi-GCM projections of future drought and climate variability indicators for the Mediterranean region. *Regional Environmental Change*, *14*(5), 1907–1919. https://doi.org/10.1007/s10113-013-0562-z

Ducrocq, V., Braud, I., Davolio, S., Ferretti, R., Flamant, C., Jansa, A., … Tamayo, J. (2014). yMeX-SOP1: The field campaign dedicated to heavy precipitation and flash flooding in the northwestern Mediterranean. *Bulletin of the American Meteorological Society*, *95*(7), 1083–1100. https://doi.org/10.1175/BAMS-D-12-00244.1

Eden, J., van Oldenborgh, G. J., Hawkins, E., & Suckling, E. B. (2015). A global empirical system for probabilistic seasonal climate prediction. *Geoscientific Model Development*, *8*(12), 3947–3973. https://doi.org/10.5194/gmd-8-3947-2015

Feldstein, S. B., & Lee, S. (2014). Intraseasonal and interdecadal jet shifts in the Northern Hemisphere: The role of warm pool tropical convection and sea ice. *Journal of Climate*, *27*, 6497–6518. https://doi.org/10.1175/JCLI-D-14-00057.1

Flaounas, E., Drobinski, P., Vrac, M., Bastin, S., Lebeaupin-Brossier, C., & Stéfanon, M. (2013). Precipitation and temperature space-time variability and extremes in the Mediterranean region: Evaluation of dynamical and statistical downscaling methods. *Climate Dynamics*, *40*(11–12), 2687–2705. https://doi.org/10.1016/j.gloplacha.2007.09.005

Furtado, J. C., Cohen, J., & Tziperman, E. (2016). The combined influences of autumnal snow and sea ice on Northern Hemisphere winters. *Geophysical Research Letters*, *43*, 3478–3485. https://doi.org/10.1002/2016GL068108

Gent, P. R., Danabasoglu, G., Donner, L. J., Holland, M. M., Hunke, E. C., Jayne, S. R., … Zhang, M. (2011). The Community Climate System Model version 4. *Journal of Climate*, *24*, 4973–4991. https://doi.org/10.1175/2011JCLI4083.1

Giorgi, F. (2006). Climate change hot-spots. *Geophysical Research Letters*, *33*, L08707. https://doi.org/10.1029/2006GL025734

Giorgi, F., & Lionello, P. (2008). Seasonal forecast of French Mediterranean heavy precipitating events linked to weather regimes. *Natural Hazards and Earth System Science*, *12*(7), 2389–2398.

Gurmy, J. F., Laanaia, N., & Cron, J. P. (2012). Climate change projections for the Mediterranean region. *Global and Planetary Change*, *63*(2–3), 90–104. https://doi.org/10.5194/nhess-12-2389-2012

Haylock, M. R., Hofstra, N., Klein Tank, A. M. G., Klok, E. J., Jones, P. D., & New, M. (2008). A European daily high-resolution gridded data set of surface temperature and precipitation for 1950–2006. *Journal of Geophysical Research*, *113*, D20119. https://doi.org/10.1029/2008JD010201

Hess, D., & Tasa, D. (2011). *McKnight's physical geography: A landscape appreciation*. Upper Saddle River, NJ: Prentice Hall.
Hoerling, M., Eischeid, J., Perlwitz, J., Quan, X., Zhang, T., & Pegion, P. (2012). On the increased frequency of Mediterranean drought. *Journal of Climate*, *25*(6), 2146–2161. https://doi.org/10.1175/JCLI-D-11-00296.1
Horton, D. E., Johnson, N. C., Sing, D., Swain, D. L., Rajaratnam, B., & Diffenbaugh, N. S. (2015). Contribution of changes in atmospheric circulation patterns to extreme temperature trends. *Nature*, *522*, 465–474. https://doi.org/10.1038/nature14550
Hwang, S.-O., Schemm, J.-K. E., Barnston, A. G., & Kwon, W. T. (2001). Long-lead seasonal forecast skill in far eastern Asia using canonical correlation analysis. *Journal of Climate*, *14*, 3005–3016. https://doi.org/10.1175/1520-0442(2001)014<3005:LLSFSI>2.0.CO;2
IPCC (2013). Climate change 2013: The physical science basis. Contribution of Working Group I to the Fifth Assessment Report of the Intergovernmental Panel on Climate Change, *Contribution of Working Group I to the Fifth Assessment Report of the Intergovernmental Panel on Climate Change*. New York, NY, USA: Cambridge University Press. http://www.ipcc.ch/report/ar5/wg1/
Kalnay, E., Kanamitsu, M., Kistler, R., Collins, W., Deaven, D., Gandin, L, … Joseph, D. (1996). The NCEP/NCAR 40-year reanalysis project. *Bulletin of the American Meteorological Society*, *77*, 437–470.
Kirtman, B. P., Min, D., Infanti, J. M., Kinter, J. L., Paolino, D. A., Zhang, Q., … Wood, F. (2014). The North American multimodel ensemble: Phase-1 seasonal-to-interannual prediction; phase-2 toward developing intraseasonal prediction. *Bulletin of the American Meteorological Society*, *95*(4), 585–601. https://doi.org/10.1175/BAMS-D-12-00050.1
Kretschmer, M., Coumou, D., Agel, L., Barlow, M., Tziperman, E., & Cohen, J. (2017). More-persistent weak stratospheric polar vortex states linked to cold extremes. *Bulletin of the American Meteorological Society*. https://doi.org/10.1175/BAMS-D-16-0259.1
Kröner, N., Kotlarski, S., Fischer, E., Lüthi, D., Zubler, E., & Schär, C. (2017). Separating climate change signals into thermodynamic, lapse-rate and circulation effects: Theory and application to the European summer climate. *Climate Dynamics*, *48*(9–10), 3425–3440. https://doi.org/10.1007/s00382-016-3276-3
Lee, S., & Feldstein, S. B. (2013). Detecting ozone- and greenhouse gas-driven wind trends with observational data. *Science*, *339*, 563–567.
Lionello, P., Bhend, J., Luterbacher, J., Buzzi, A., Della-Marta, P. M., & Krichak, S. O. (2006). Cyclones in the Mediterranean region: Climatology and effects on the environment. *Developments in Earth and Environmental Sciences*, *4*, 325–372. https://doi.org/10.1016/S1571-9197(06)80009-1
Lionello, P., Piero, P. M.-R., & Boscolo, R. (2006). *Mediterranean climate variability* (p. 4). Amsterdam, Netherlands: Elsevier.
Merryfield, A., Lee, W.-S., Boer, G. J., Kharin, V. V., Scinocca, J. F., Flato, G. M., … Fyfe, J. C. (2013). The Canadian seasonal to interannual prediction system. Part I: Models and initialization. *Monthly Weather Review*, *141*, 2910–2945. https://doi.org/10.1175/MWR-D-12-00216.1
Mariotti, A., Pan, Y., Zeng, N., & Alessandri, A. (2015). Long-term climate change in the Mediterranean region in the midst of decadal variability. *Climate Dynamics*, *44*, 1437–1456. https://doi.org/10.1007/s00382-015-2487-3
Mbengue, C., & Schneider, T. (2013). Storm track shifts under climate change: What can be learned from large-scale dry dynamics. *Journal of Climate*, *26*(24), 9923–9930. https://doi.org/10.1175/JCLI-D-13-00404.1
Paeth, H., Vogt, G., Paxian, A., Hertig, E., Seubert, S., & Jacobeit, J. (2017). Quantifying the evidence of climate change in the light of uncertainty exemplified by the Mediterranean hot spot region. *Global and Planetary Change*, *151*, 144–151. https://doi.org/10.1016/j.gloplacha.2016.03.003
Park, S., & Leovy, C. B. (2004). Marine low-cloud anomalies associated with ENSO. *Journal of Climate*, *17*(17), 3448–3469. https://doi.org/10.1175/1520-0442(2004)017<3448:MLAAWE>2.0.CO
Rayner, N. A., Parker, D. E., Horton, E. B., Folland, C. K., Alexander, L. V., Rowell, D. P., … Kaplan, A. (2013). Global analyses of sea surface temperature, sea ice, and night marine air temperature since the late nineteenth century. *Journal of Geophysical Research: Atmospheres*, *108*, 3448—3469. https://doi.org/10.1029/2002JD002670
Robinson, D. A., Estilow, W. T., & NOAA CDR PrograM (2012). *NOAA Climate Date Record (CDR) of Northern Hemisphere (NH) Snow Cover Extent (SCE), version 1*. Maryland, USA: NOAA National Climatic Data Center. https://doi.org/10.7289/V5N014G9
Saha, S., Wu, X., Wang, J., Nadiga, S., Tripp, P., Behringer, D., … Becker, E. (2014). The NCEP climate forecast system version 2. *Journal of Climate*, *27*, 4655–4676. https://doi.org/10.1175/JCLI-D-13-00446.1
Shaman, J., & Tziperman, E. (2011). An atmospheric teleconnection linking ENSO and southwestern European precipitation. *Journal of Climate*, *24*(1), 124–139. https://doi.org/10.1175/2010JCLI3590.1
Smithson, P., Addison, K., & Atkinson, K. (2013). *Fundamentals of the physical environment*. London: Routledge.
Ullbrich, U., May, W., Li, L., Lionelle, P., Pinto, J. G., & Somot, S. (2006). The Mediterranean climate change under global warming. *Developments in Earth and Environmental Sciences*, *4*, 399–415. https://doi.org/10.1016/S1571-9197(06)80011-X
Weisheimer, A., & Palmer, T. N. (2014). On the reliability of seasonal climate forecasts. *Journal of the Royal Society, Interface*, *11*(96), 20131162. https://doi.org/10.1098/rsif.2013.1162
Wilks, D. S. (2011). *Statistical methods in the atmospheric sciences* (pp. 100). Waltham, USA: Academic Press.
Xoplaki, E., Gonzalez-Rouco, J. F., Luterbacher, J., & Wanner, H. (2004). Wet season Mediterranean precipitation variability: Influence of large-scale dynamics and trends. *Journal of Climate*, *23*(1), 63–78. https://doi.org/10.1007/s00382-004-0422-0
Yatagai, E. A., Krishnamurti, T. N., Kumar, V., Mishra, A. K., & Simon, A. (2014). Use of APHRODITE rain gauge based precipitation and TRMM 3B43 products for improving Asian monsoon seasonal precipitation forecasts by the superensemble method. *Journal of Climate*, *27*(3), 1026–1069. https://doi.org/10.1175/JCLI-D-13-00332.1

Supporting Information for "Winter precipitation forecast in the European and Mediterranean regions using cluster analysis"

Sonja Totz[1,2], Eli Tziperman[3], Dim Coumou[1,4], Karl Pfeiffer[5], and Judah Cohen[5]

[1]Potsdam Institute for Climate Impact Research, Potsdam, Germany

[2]Department of Physics, University of Potsdam, Germany

[3]Department of Earth and Planetary Sciences, and School of Engineering and Applied Sciences, Harvard University, Cambridge, Massachusetts

[4]Institute for Environmental Studies (IVM), VU University Amsterdam

[5]Atmospheric and Environmental Research, Inc., Lexington, Massachusetts 02421, USA

Contents of this file:

1. Introduction

The supplemental information contains a description of the clustering-based prediction approach, a demonstration of the method using a simple toy problem and a comparison to standard regression-based prediction, and eleven additional figures to provide more information of our cluster-based forecast method as applied to the Mediterranean precipitation problem.

2. Cluster-based prediction methodology

Given the time series of the quantity to be predicted (predictand, e.g., anomaly winter (DJF) precipitation) and precursors (predictors, e.g., autumn (SON) sea ice cover and snow cover extent), we calculate the clusters of the predictand, and then use them to construct the prediction, as shown schematically in Fig. S8 and described as follows. Consider a forecast of precipitation anomaly time series at several locations, given by the predictand vector $\mathbf{prcp}(t)$. These precipitation data will be predicted using given precursors, e.g., time series of snow cover extent at several spatial locations given by the time-dependent vector $\mathbf{sce}(t)$, and time series of sea ice extent at several spatial locations, $\mathbf{sic}(t)$.

We assume that there are $N_{clusters}$ significant precipitation clusters. We use bold upper case variable names to denote clusters and composites, and lower case bold variable names to denote time series data. The prediction procedure requires the winter (DJF) precipitation clusters $\mathbf{PRCP}_i$, $i = 1, \ldots, N_{clusters}$ and the corresponding precursor composites (e.g., sea ice cover and snow cover extent anomalies from the autumn SON mean), $\mathbf{COMPOSITE}_i$. The clusters are calculated using hierarchical clustering of the winter precipitation anomaly data, while the composites for a given cluster i are calculated by averaging the predictors over all times in which the precipitation anomaly is assigned to its cluster i.

We also need a time series of the autumn-mean (averaged over SON) precursor anomaly (predictors) $\mathbf{precursor}_{SON}(t)$, for each spatial location. The time t denotes the year, where the precursors are evaluated during the fall (SON) and the precipitation of that year refers to the following DJF. For example, if the precursors are sea ice and snow cover, the vector of precursors (predictors) time series, and the vector of composites are calculated as follows,

$$\begin{aligned}
\mathbf{precursor}_{SON}(t) &= (\mathbf{sic}_{SON}(t), \mathbf{sce}_{SON}(t))^T \\
\mathbf{COMPOSITE}_{1,2} &= (\mathbf{SIC}_{1,2}, \mathbf{SCE}_{1,2})^T
\end{aligned}$$

To obtain the prediction for the precipitation, we first find the projection of the current state of the predictors (snow cover and sea ice) on the $N_{clusters}$ predictor composites corresponding to the precipitation clusters. Each predictor composite is associated with a precipitation cluster and provides information about the amplitude and spatial structure of winter precipitation expected given the autumn predictor composite. This allows us to calculate the expected precipitation pattern due to the projection of the current state of predictors on each cluster. Finally, we sum the contributions to the precipitation due to all clusters, to obtain the predicted total precipitation anomaly.

Mathematically, this proceeds as follows. To calculate the projection of $\mathbf{precursor}_{SON}(t)$ on the composite $\mathbf{COMPOSITE}_i$, we expand the current precursor state in terms of the precursor composites, to find the expansion coefficients, noting that the composites are not necessarily orthogonal. The expansion takes the form,

$$\mathbf{precursor}_{SON}(t) \approx \sum_{i=1}^{N_{clusters}} a_i(t)\ \mathbf{COMPOSITE}_i.$$

The expansion may only be approximate because the composites are not necessarily a complete set of vectors. To find the expansion coefficients $a_i(t)$, multiply by precursor composite $\mathbf{COMPOSITE}_j$, remembering that they are not necessarily orthogonal,

$$\mathbf{precursor}_{SON}(t) \cdot \mathbf{COMPOSITE}_j = \sum_{i=1}^{N_{clusters}} a_i(t)\ \mathbf{COMPOSITE}_i \cdot \mathbf{COMPOSITE}_j.$$

Next, we write this as a matrix equation for the unknown vector $\mathbf{a}(t)$ of coefficients $a_i(t)$. Define a matrix, $B_{ij} = \mathbf{COMPOSITE}_i \cdot \mathbf{COMPOSITE}_j$, and the right-hand side $\mathbf{\Gamma}_j(t) = \mathbf{precursor}_{SON}(t) \cdot \mathbf{COMPOSITE}_j$. This leads to the linear equations,

$$B\ \mathbf{a}(t) = \mathbf{\Gamma}(t),$$

that may be solved for the coefficients $a_i(t)$ at every time step (year t) in the data. Given that the matrix B may be ill conditioned, there may be many solutions for $\mathbf{a}(t)$. We choose the one with the smallest norm, using the SVD-based pseudo inverse.

The final expression for the predicted precipitation is obtained by summing the contribution of all clusters, each multiplied by the projection of the current state of precursors, $a(i)$,

$$\mathbf{prcp}(t) = \sum_{i=1}^{N_{clusters}} a_i(t)\ \mathbf{PRCP}_i. \tag{1}$$

3. Demonstrating the clustering-based prediction approach using a toy problem

We now consider a toy problem to demonstrate the clustering-based forecast approach used in the main paper to predict precipitation, and to test it against a commonly used regression-based prediction model. We first create test data for this demonstration problem that are characterized by a specified cluster structure (section 3.1). Next, we present the regression prediction results (section 3.2), and discuss the difference between the two (section 3.3). We emphasize that the intent of the comparison is not to show the superiority of the clustering or regression approaches, but only to explain the difference between the two methods.

3.1. Creating the data

For this toy problem demonstration of the methodology, we consider a forecast of precipitation anomaly time series at three locations, given by the predictand vector $\mathbf{prcp}(t)$. These precipitation data will be predicted using two precursors: time series of snow cover extent at two spatial locations given by the time-dependent vector $\mathbf{sce}(t)$, and time series of sea ice extent at two spatial locations, $\mathbf{sic}(t)$.

Normally, one would start applying this prediction approach by clustering the precipitation data and then calculating the predictor composites. In order to demonstrate this approach in the simplest possible scenario, we instead create a data set with a specified structure for the precipitation clusters and precursor composites, and create corresponding time series for both the precipitation and precursors vectors.

We start by specifying two winter precipitation anomaly clusters,

$$\begin{aligned}\mathbf{PRCP}_1 &= (p_1, p_2, p_3)^T = (1, -1, 1)^T \\ \mathbf{PRCP}_2 &= (p_1, p_2, p_3)^T = (1, 1, -1)^T\end{aligned}$$

The first cluster, for example, implies that the precipitation anomaly in the first location is inversely correlated with that in the second location. We associate with these precipitation clusters the following specified composites of snow cover and sea ice extent,

$$\begin{aligned}\mathbf{SCE}_1 &= (-1, 1)^T \\ \mathbf{SCE}_2 &= (-1, 0)^T \\ \mathbf{SIC}_1 &= (1, -1)^T \\ \mathbf{SIC}_2 &= (1, 1)^T, \end{aligned} \tag{2}$$

such that $\mathbf{SCE}_1$, for example, is the snow cover extent anomaly at two locations, corresponding to the first precipitation anomaly cluster: when the snow cover extent has the structure of $\mathbf{SCE}_1$, we expect the precipitation anomaly to have the structure given by $\mathbf{PRCP}_1$. In order to create the time series data for predictors and predictands that are characterized by the specified clusters, we first create a matrix A that relates the precursor composites to the precipitation clusters,

$$\mathbf{PRCP}_i \;=\; A\,\mathbf{COMPOSITE}_i. \tag{3}$$

This matrix is given by,

$$A \;=\; \begin{pmatrix} 1 & 2 & 1 & 1 \\ -1/2 & 0 & -1/2 & 1 \\ -1 & 0 & -1 & -1 \end{pmatrix}.$$

We next construct the following idealized time behavior for the two precursors, by adding noise to their specified composite structure $\mathbf{COMPOSITE}_i$, as follows,

$$\mathbf{precursor}_{SON}(t) \;=\; \mathcal{D}\left(\mathbf{COMPOSITE}_i, \sigma, t\right),$$

where $\mathcal{D}$ is a multivariate Gaussian random distribution with a mean $\mathbf{COMPOSITE}_i$ and root mean square (RMS) equal to σ. Effectively this means that at every time t, one of the composites is selected with some added noise. We construct these time series for $N = 1000$ years.

Given the time series of the precursors, $(\mathbf{sce}_i(t), \mathbf{sic}_i(t))$, we can calculate the time series of the precipitation for this toy problem, using a two-step procedure. First, we use the same matrix used in (3) to relate the precursor composites to the precipitation clusters, in order to estimate the precipitation signal due to cluster i, as forced by precursors $\mathbf{sce}_i(t), \mathbf{sic}_i(t)$. This signal is equal to the matrix A times the ith precursor. Next, we sum over the precipitation of all clusters (two of them in this example), to get the total precipitation at a time t. The result for the precipitation vector time series representing the precipitation anomaly at four locations is,

$$\mathbf{prcp}(t) = A\;\mathbf{precursor}_{SON}(t).$$

Fig. S1 shows the time series for the two sea ice cover precursors, two snow cover extent precursors, and scatter plots for the precipitation, snow cover and sea ice data showing the cluster structure.

3.2. Regression model

In a standard regression-based prediction scheme, the prediction for the winter (DJF) precipitation anomaly at location i, as function of time, $\mathrm{prcp}_i(t)$, is written as a linear function of the precursors (SON sea ice and snow cover) plus a noise term,

$$\mathrm{prcp}_i(t) = \mathbf{a}_i \cdot \mathbf{sce}(t) + \mathbf{b}_i \cdot \mathbf{sic}(t) + \xi.$$

One then finds the regression coefficients (both vectors) $\mathbf{a}_i, \mathbf{b}_i$ that minimize the distance to the observed precipitation at each location at all times. However, in practice, involving all grid points of the precursors requires to find many regression coefficients using insufficient number of observations and therefore results in an over-fitting problem. One therefore tries to reduce the number of regression coefficients that need to be calculated by using only, for example, the average of each precursor. In our example, one would use the average sea ice extent over all locations and the average snow cover over all locations. This would require to find only two regression coefficients for each precipitation location instead of four. The regression model then takes the form,

$$\mathrm{prcp}(t)_i = a_i \ \overline{\mathrm{sce}}(t) + b_i \ \overline{\mathrm{sic}}(t) + \xi$$

where $\overline{\mathrm{sce}}(t)$ and $\overline{\mathrm{sic}}(t)$ are the averages of each precursor over all grid points.

3.3. Comparing the cluster-based forecast method and the regression model

We now apply the clustering-based prediction method described in section 2 and the regression based approach described in section 3.2 to the data created as described in section 3.1. The forecast calculated with the cluster-based method coincides well with the "observations" (compare black and red lines in Fig. S2). This is to be expected, as the "observations" were created using only two clusters, and these clusters therefore lead to good predictability. In contrast, the forecast obtained using the regression model fails in Figs. S2b and S2c. The regression fails here, simply because our indices reflecting the average of sea ice for both grid points and the average of snow cover for both grid points are not appropriate indices. Specifically, the average cannot represent the first snow cover cluster structure and the first sea ice cluster structure seen in Eqn. (1).

We emphasize that this is not meant to be a test for the clustering vs regression approaches, as the "observations" are, by construction, optimally suited for the clustering-based prediction approach, and the predictor indices for the regression approach are poorly chosen. Rather, the purpose here is only to explain the difference between the two methods.

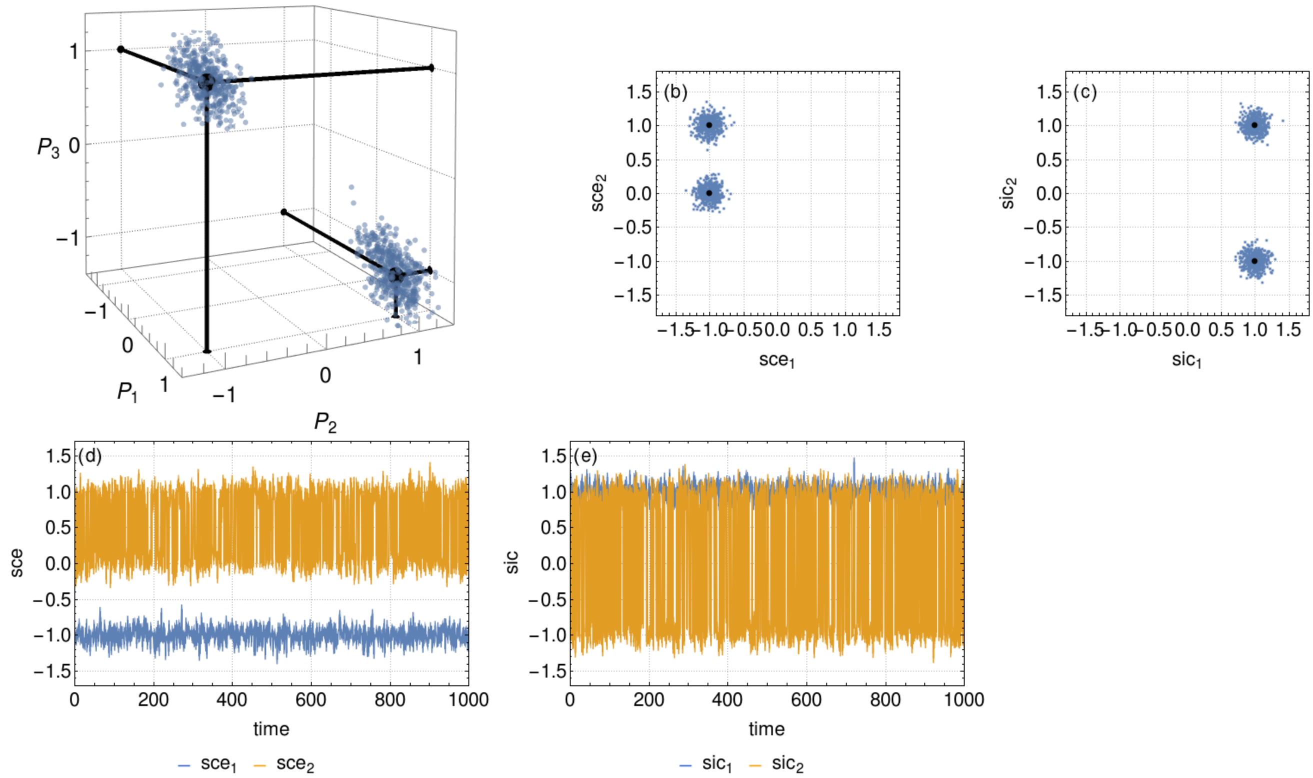

Figure S1. (a) 3D scatter plot of precipitation data in toy model, with black dots showing the clusters. Each axis represents one the precipitation anomaly of one location. (b) 2d scatter plot of sea ice concentration for all data points, (c) 2d scatter plot of snow cover extent for all data points. Each axes represents only sce anomaly (sic anomaly) of one location. (d) Time series of sea ice data at two locations represented by blue and yellow solid lines. (e) Time series of snow cover extent at two locations represented by blue and yellow solid lines.

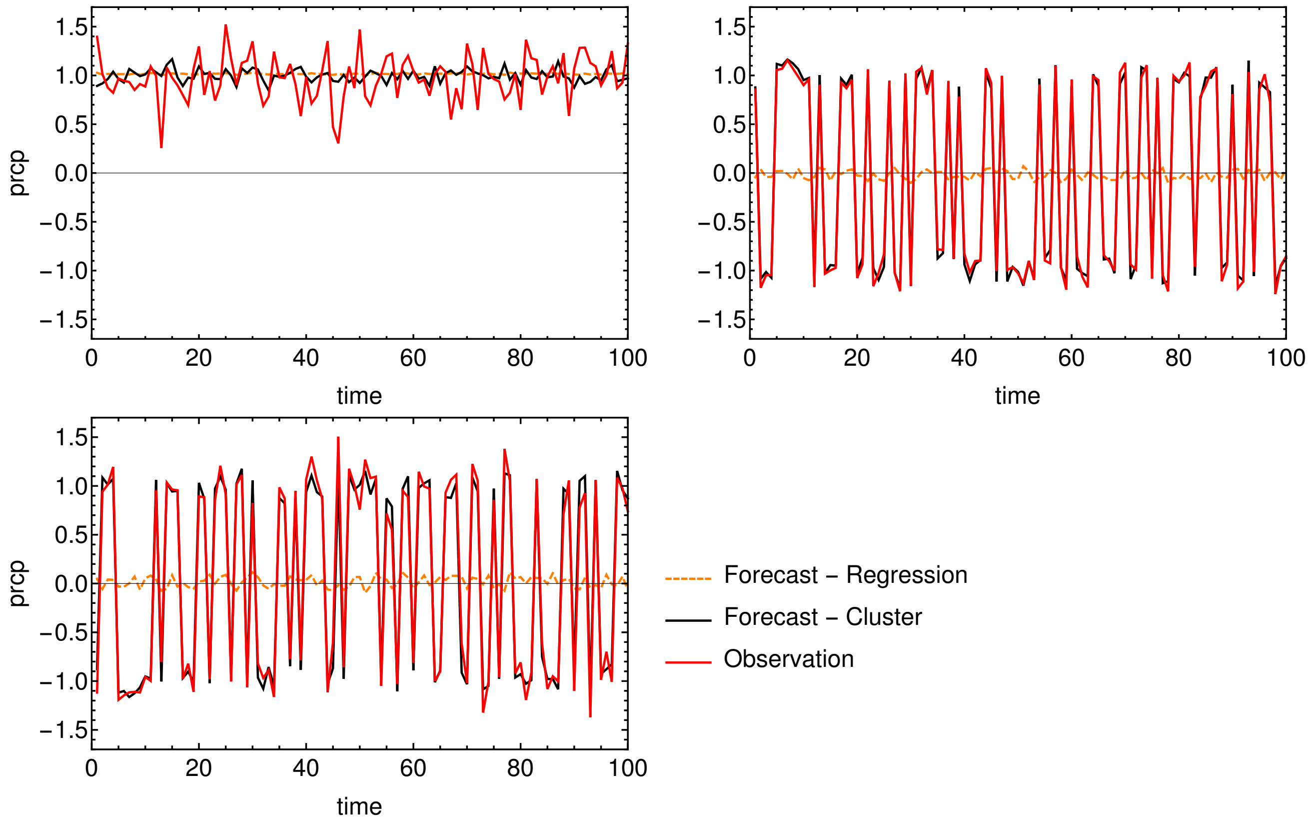

Figure S2. Precipitation anomalies vs prediction using the clustering-based and regression-based approaches. Red lines represent the artificially created precipitation anomalies, black line show the forecast calculated using the cluster-based method, and dashed orange lines show the forecast calculated by a regression model. In subplots (b) and (c) the regression forecast fails.

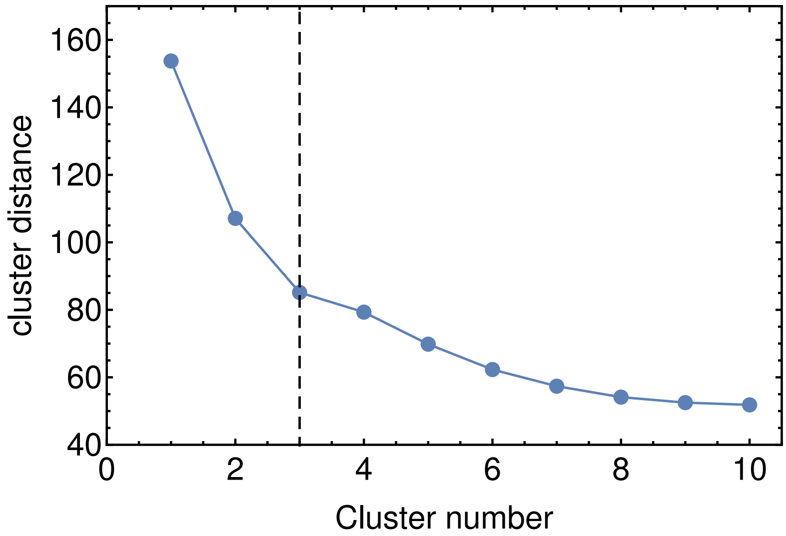

Figure S3. Elbow-plot of hierarchical clustering with precipitation anomalies of the Mediterranean region. Only the last 10 steps of the clustering are shown. The blue line represents the cluster distance. A kink of the cluster distance indicates the optimal number of clusters.

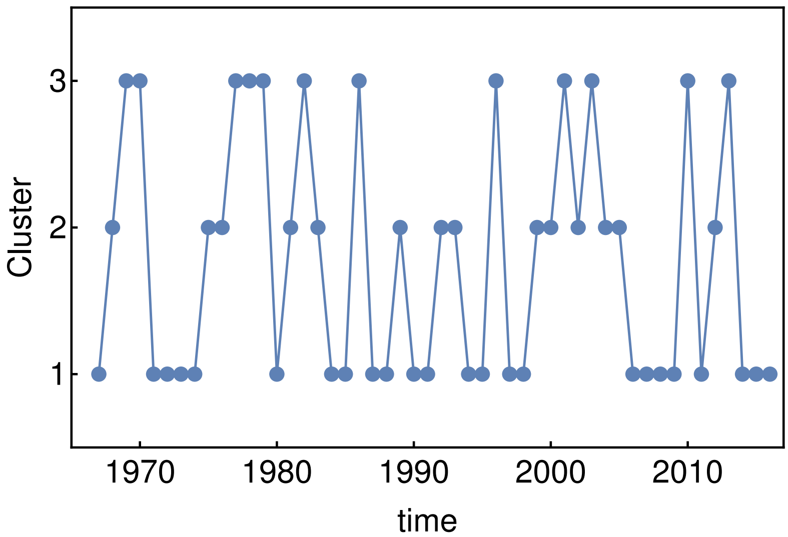

Figure S4. Cluster-time-plot of the four precipitation anomaly clusters between 1967-2016. Cluster one appears most often, cluster two is the second most important cluster and cluster three appears the least likely ocurred cluster.

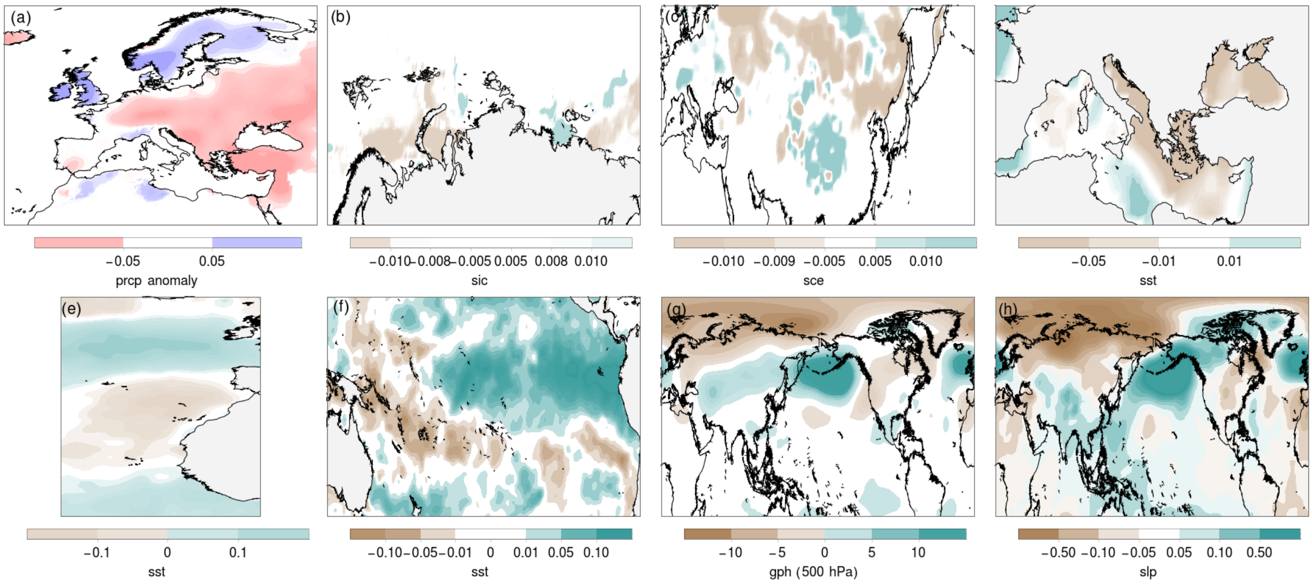

Figure S5. (a) precipitation anomaly of cluster one. Composite mean of sea ice concentration anomalies (b) , snow cover extent anomalies (c), sea surface temperature anomalies in the Mediterranean region (d), sea surface temperature anomalies in the Atlantic region (e), sea surface temperature anomalies in the Pacific region (f),sea surface temperature anomalies in the South Pacific, geopotential height anomalies at 500mb (g) and sea level pressure anomalies (h) over all autumn seasons that were assigned to cluster one.

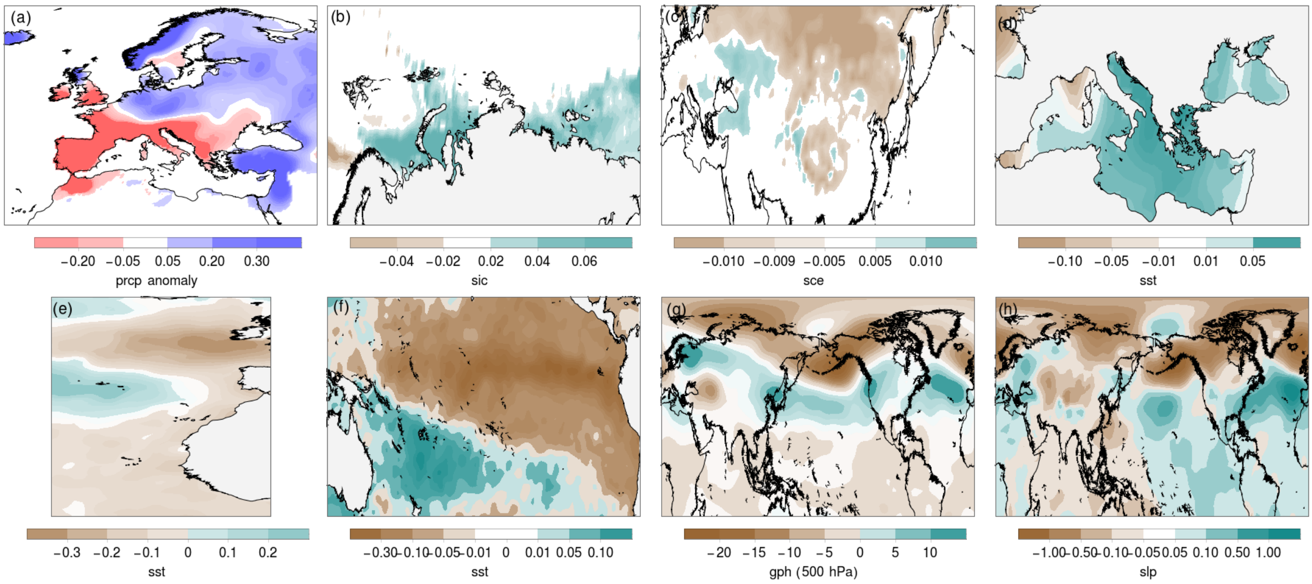

Figure S6. (a) precipitation anomaly of cluster two. (b-h) composites over all autumn seasons that were assigned to cluster two (compare Fig. S1).

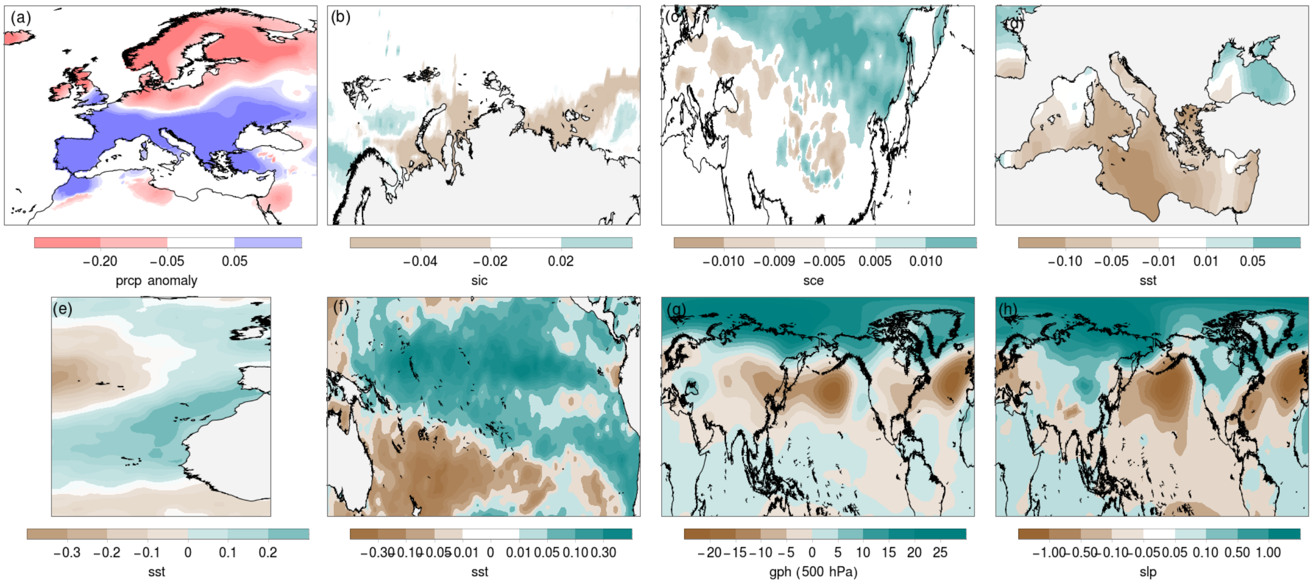

Figure S7. (a) precipitation anomaly of cluster three. (b-h) composites over all autumn seasons that were assigned to cluster three (compare Fig. S1).

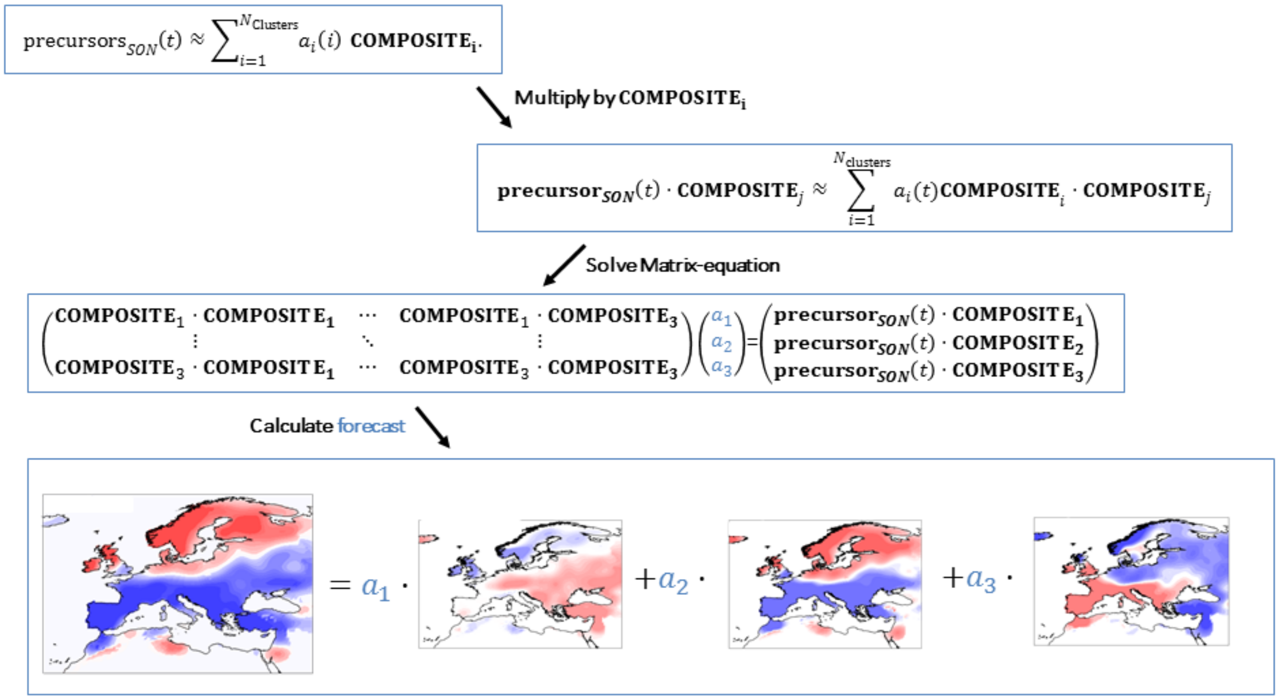

Figure S8. Forecast scheme. First the precursors are expanded in terms of the composites. In the next step, the equation is multiplied by another composite. The resulting matrix equation is solved using the SVD-based pseudo-matrix to find the expansion coefficients. Finally, the forecast is calculated by the expansion coefficients and the precipitation anomaly clusters.

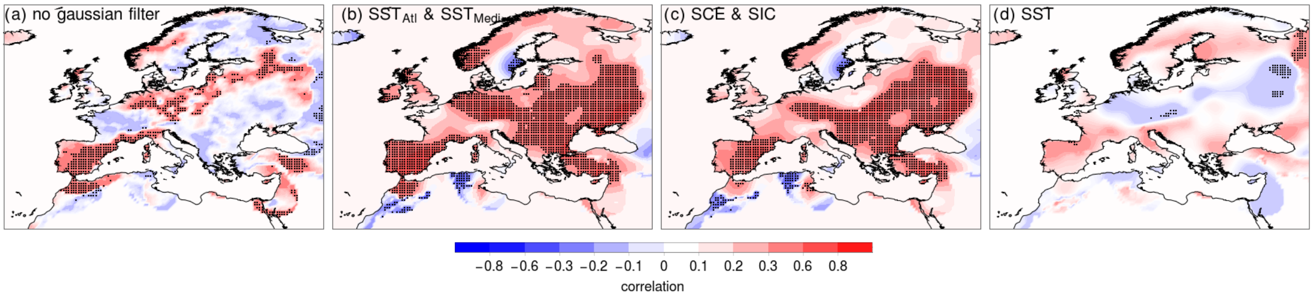

Figure S9. (a) Cross-validated correlation of the cluster forecast method for the years 1967 - 2016 without the Gaussian filter. (b) Cross-validated correlation of the cluster forecast method for the years 1967 - 2016, considering sea surface temperature in the Mediterranean region and Atlantic region as precursors. (c) Cross-validated correlation of the cluster forecast method for the years 1967 - 2016, considering sea ice concentration and snow cover extent as precursors. (d) Cross-validated correlation of the cluster forecast method for the years 1967 - 2016, considering sea surface temperature in the Mediterranean region, in the tropics and the Atlantic as precursors. Significant values ($P<0.05$) according to two-sided Student's t-test are shown in hatches.

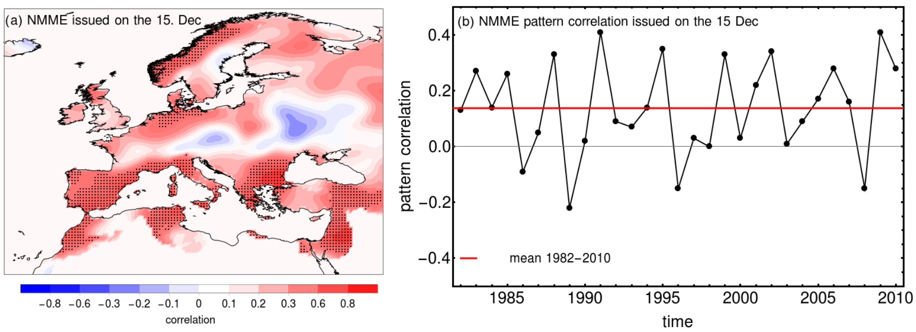

Figure S10. Cross-validated correlation of the DJF NMME hindcast for the years 1982 - 2010 issued on the initial conditions from December 15th. (b) Pattern correlation of the precipitation DJF NMME hindcast between 1982−2010 issued on initial conditions from December 15th. The black line is the pattern correlation and the red solid line is the mean pattern correlation.